LANGMUIR APPLICATIONS LIST - [LP17]

Impedans
PLASMA MEASUREMENT

LANGMUIR PROBE SYSTEM

The Impedans' Langmuir Probe system is used by academia and industry globally for plasma characterisation. Below is a list of publications with their plasma sources, process gases, pressures and applications.

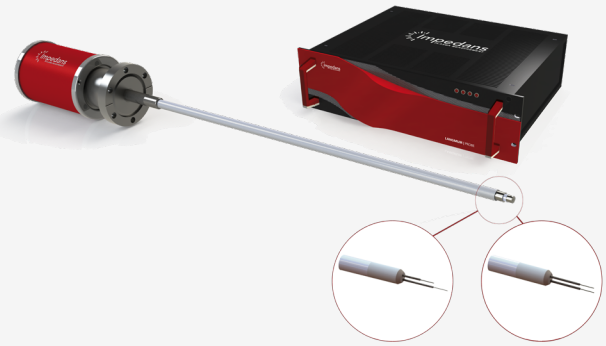

Plasma Source	Density (m^{-3})	Gas	Pressure(mTorr)	Published Paper
2.45 GHz MW	10^{11} -> 10^{15}	N_2 ,N_2,O_2	6000	Electrical characterization of the flowing afterglow of N2 and N2/O2 microwave plasmas at reduced pressure
CCP	10^{14} -> 10^{15}	Ar+C	11.3	Suppression of a spontaneous dust density wave by a modulation of ion streaming
CCP	10^{15} -> 10^{16}	Ar	60 -> 400	Plasma parameters of RF capacitively coupled discharge comparative study between a plane cathode and a large hole
CCP	10^{16}	-	<75	Analysis of double-probe characteristics in low-frequency gas discharges and its improvement
CCP	10^{15}	N_2	100 -> 1000	Capacitively coupled radio frequency nitrogen plasma generated at two different exciting frequencies of 13.56 MHz and 40 MHz analyzed using Langmuir probe along with optical emission
CCP	10^{16} -> 10^{17}	Ar	200 -> 500	Plasma parameters in 40 MHz Argon discharge
Hall Thruster	10^{15} -> 10^{18}	Xe	13.5 -> 45	Anode geometry influence on LaB6 cathode discharge characteristics
Hall Thruster	10^{15} -> 10^{16}	Ar	30	Measurement of plasma parameters in the far-field plume of a Hall effect thruster
Hall Thruster	10^{16} -> 10^{17}	Xe	0.0015	Electron flow properties in the far-field plume of a Hall thruster
Hall Thruster	10^{15} -> 10^{16}	Xe,Kr	0.0225	Time-resolved measurement of plasma parameters in the far-field plume of a low-power Hall effect thruster
Hall Thruster	10^{16}	Xe	0.015	The time-varying electron energy distribution function in the plume of a Hall thruster
Hall Thruster	10^{16} -> 10^{18}	Xe	0.015	Electron energy distribution function in a low-power Hall thruster discharge and near-field plume
Helicon	10^{16} -> 10^{17}	Ar	2.6	Two density peaks in low magnetic field helicon plasma
Helicon	10^{15} -> 10^{16}	Ar	2.62	Modulation of absorption manner in helicon discharges by changing profile of low axial magnetic field*
HiPIMS	10^{16} -> 10^{17}	Ar,Cr	0.5 -> 20	Spectroscopic investigation on the near-substrate plasma characteristics of chromium HiPIMS in low density discharge mode
HiPIMS	10^{13} -> 10^{17}	Ar,O_2,Ti	6.98	The behaviour of negative oxygen ions in the afterglow of a reactive HiPIMS discharge
HiPIMS	10^{16} -> 10^{18}	Ar,O_2,Ti	5.63	Design of magnetic field configuration for controlled discharge properties in highly ionized plasma
HiPIMS	10^{15} -> 10^{16}	Ar,O_2,Al	1.5	Investigating the plasma parameters and discharge asymmetry in dual magnetron reactive high power impulse magnetron sputtering discharge with Al in Ar/O2 mixture

HiPIMS	10^{16} -> 10^{17}	Ar,O_2,Ti	7.5	Angular dependence of plasma parameters and film properties during high power impulse magnetron sputtering for deposition of Ti and TiO2 layers
HiPIMS	10^{16} -> 10^{18}	Ar,O_2,Ti	5.63	Enhanced oxidation of TiO2 films prepared by high power impulse magnetron sputtering running in metallic mode
HiPIMS - ECWR	< 10^{18}	Ar,O_2,Ti	0.6 -> 75	Deposition of rutile (TiO2) with preferred orientation by assisted high power impulse magnetron sputtering
HiPIMS - ECWR	10^{16} -> 10^{18}	Ar,Ti	0.375	Plasma diagnostics of low pressure high power impulse magnetron sputtering assisted by electron cyclotron wave resonance plasma
Hot Cathode Magnetic Filter	10^{11} -> 10^{12}	Ar,SF_6	0.165	Sheath characteristics in a magnetically filtered low density low temperature multicomponent plasma with negative ions
Hot Cathode Plasma	10^{13}	Ar	0.8	Matched dipole probe for magnetized low electron density laboratory plasma diagnostics
Hot Cathode Plasma	10^{12} -> 10^{13}	Ar	0.15	Ion and electron sheath characteristics in a low density and low temperature plasma
Hybrid – Dual- HiPIMS	10^{17} -> 10^{18}	Ar,Ti,Cu	3 -> 30	Time-resolved Langmuir probe investigation of hybrid high power impulse magnetron sputtering discharges
ICP	10^{17}	H	3.75 -> 22.5	Investigation of the power transfer efficiency in a radio-frequency driven negative hydrogen ion source
ICP	10^{17} -> 10^{18}	Ar	3.75 -> 75	Nonlocal electron kinetics and spatial transport in radio-frequency two-chamber inductively coupled plasmas with argon discharges
ICP	10^{16}-> 10^{17}	Ar,	10 -> 50	A hybrid model of radio frequency biased inductively coupled plasma discharges: description of model and experimental validation in argon
ICP	10^{16}-> 10^{17}	Ar,O_2	10 -> 50	Experimental and numerical investigations on time-resolved characteristics of pulsed inductively coupled O2/Ar plasmas
ICP	10^{15}-> 10^{17}	H,Ar	2 -> 150	Investigation of a Magnetically Enhanced Inductively Coupled Negative Ion Plasma Source
Magnetic Mirror	10^{16}-> 10^{17}	N_2	0.2 -> 4	Signatures of ring currents in a magnetic mirror plasma experiment
Magnetron	10^{16}-> 10^{17}	Ar,Cu	0.75 -> 37.5	The erosion groove effects on RF planar magnetron sputtering
Magnetron	2 -> 70 A/m^2	Ar,N_2,Al	3.75	Tunable ion flux density and its impact on AlN thin films deposited in a confocal DC magnetron sputtering system
MAGPIE	10^{16} -> 10^{17}	Ar	1.4 -> 3	Plasma parameters and electron energy distribution functions in a magnetically focused plasma.
MAGPIE	10^{16} -> 10^{17}	H	5 -> 10	Negative hydrogen ion production in a helicon plasma source
MAGPIE	< 10^{19}	H	10	Ion flux dependence of atomic hydrogen loss probabilities on tungsten and carbon surfaces
MW	10^{14}	Ar	150 -> 200	Apparatus for generating quasi-free-space microwave-driven plasmas
NExET	10^{18}	Xe	-	Anode position influence on discharge modes of a LaB6 cathode in diode configuration
PEGASES Thruster	10^{18}	SF_6,Ar,Xe, He,O_2,N_2	0.75	Plasma drift in a low-pressure magnetized radio frequency discharge
Proton Linear Accelerator	10^{18} -> 10^{19}	H	1.125 -> 5	Plasma characterization of the superconducting proton linear accelerator plasma generator using a 2 MHz compensated Langmuir probe
Pulsed Laser Deposition	10^{16}	O_2,WO_3	7.5	Optimization of substrate-target distance for pulsed laser deposition of tungsten oxide thin films using Langmuir probe
Pulsed Laser Deposition	10^{16} -> 10^{17}	O_2,CeO_2	7.5	Plasma plume behavior of laser ablated cerium oxide: Effect of oxygen partial pressure
PULVA reactor	10^{15}	Ar,C_2H_2	15 -> 30	Metastable argon atom density in complex argon/acetylene plasmas determined by means of optical absorption and emission spectroscopy
VHF Multi-tile Push-Pull	10^{16} -> 10^{17}	N_2	5 -> 25	Nitriding process for next-generation semiconductor devices by VHF (162 MHz) multi-tile push-pull plasma source

HiPIMS	10^{15} -> 10^{16}	Ar,O_2,Al	1.5	Investigating the plasma parameters and discharge asymmetry in dual magnetron reactive high power impulse magnetron
Helicon	10^{15} -> 10^{16}	Ar	2.62	Modulation of absorption manner in helicon discharges by changing profile of low axial magnetic field*
Magnetron	2 -> 70 Am^{-2}	Ar,N_2,Al	3.75	Tunable ion flux density and its impact on AlN thin films deposited in a confocal DC magnetron sputtering system
HiPIMS	10^{16} -> 10^{17}	Ar,O_2,Ti	7.5	Angular dependence of plasma parameters and film properties during high power impulse magnetron sputtering for deposition of Ti and TiO2 layers
ICP	10^{16} -> 10^{17}	Ar,O_2	10 -> 50	Experimental and numerical investigations on time-resolved characteristics of pulsed inductively coupled O2/Ar plasmas
HiPIMS	10^{16} -> 10^{18}	Ar,O_2,Ti	5.63	Enhanced oxidation of TiO2 films prepared by high power impulse magnetron sputtering running in metallic mode
Hot Cathode Plasma	10^{13}	Ar	0.8	Matched dipole probe for magnetized low electron density laboratory plasma diagnostics
Hall Thurster	10^{16} -> 10^{18}	Xe	0.015	Electron energy distribution function in a low-power Hall thruster discharge and near-field plume
CCP	10^{16} -> 10^{17}	Ar	200 -> 500	Plasma parameters in 40 MHz Argon discharge
Hot Cathode Plasma	10^{12} -> 10^{13}	Ar	0.15	Ion and electron sheath characteristics in a low density and low temperature plasma
ICP	10^{15} -> 10^{17}	H,Ar	2 -> 150	Investigation of a Magnetically Enhanced Inductively Coupled Negative Ion Plasma Source
Hollow Cathode	10^{15} -> 10^{18}	O_2	450 -> 825	Characterization and application of hollow cathode oxygen plasma
ICP	10^{17}	H	2.25	Development of RF Driver Used in Negative Ion Source at HUST
CCP	10^{16} -> 10^{17}	Ar	525 -> 862	The Study of plasma parameters and the effect of experiment set up modification by using modelling software
ICP	10^{16}	H	45	Study on the RF Power Necessary to Ignite Plasma for the ICP Test Facility at HUST
ECR	10^{14} -> 10^{16}	Ar,Air	3 -> 75	2.45 GHz ECR coaxial plasma source: characterization in single and multi-sources configuration
Helicon	10^{16} -> 10^{18}	Ar	2.25	The Evolution of Discharge Mode Transition in Helicon Plasma Through ICCD Images
Dual-Hybrid HiPIMS	10^{15} -> 10^{18}	Ar, Cu, Ti	2.25	Deposition of nanostructured Cu-Ti based films by advanced magnetron sputtering methods
CCP	10^{15} -> 10^{16}	Ar, N_2	100 -> 1000	Synthesis and characterization of fluorene-type and hydrogenated amorphous carbon thin films in RF and DC glow
Dual CCP	10^{12} -> 10^{15}	N_2	100 -> 1000	Surface modification of unsized pan-based carbon fiber by using high frequency single and dual RF discharge system
Dual CCP	10^{13} -> 10^{15}	N_2	100 -> 700	Investigation of Single and Dual RF Capacitively Coupled Nitrogen Plasma Discharges Using Optical Emission
PEGASES Thruster	10^{15} -> 10^{17}	Ar,Xe	0.75	Investigation of Magnetized radio frequency plasma courses for electric space propulsion
ICP	10^{15}	Ar	2 -> 10	Comparison of plasma parameters determined with a Langmuir probe and with a retarding field energy analyzer
Hollow Cathode	10^{16}	Ar, Air	375 -> 750	Probe Diagnostics of Plasma Parameters in a Large-Volume Glow Discharge With Coaxial Gridded Hollow Electrodes
Hollow Cathode	10^{15} -> 10^{16}	Ar	187.5	Numerical and Experimental Diagnostics of Dusty Plasma in a Coaxial Gridded Hollow Cathode Discharge
CCP	10^{15}	He,O_2	40 ml/min - 80 ml/min	An investigation on optical properties of capacitive coupled radio-frequency mixture plasma with Langmuir probe
Hollow Cathode	10^{16}	Ar	187.5	Investigation of Low-Pressure Glow Discharge in a Coaxial Gridded Hollow Cathode
CCP	10^{14} -> 10^{15}	Ar,H_2	75 -> 240	Comments on the Langmuir probe measurements of radio-frequency capacitive argon–hydrogen mixture discharge at low pressure

MW	10^{15} -> 10^{16}	He	525	Microwave technology used for plasma diagnostic in complicated situations
Dual-Hybrid HiPIMS	10^{17} -> 10^{18}	Ar,Cu,Ti	3 -> 30	Time-resolved Langmuir probe investigation of hybrid high power impulse magnetron sputtering discharges
Hollow Cathode	10^{16}	He	112.5	Diagnostics of large volume coaxial gridded hollow cathode DC discharge
Hollow Cathode	10^{16} -> 10^{17}	He	112.5 -> 562.5	Broadband microwave propagation in a novel large coaxial gridded hollow cathode helium plasma
Pulsed ICP	10^{15} -> 10^{16}	CH_4,O_2,Ar	0.975	Nanometer-scale etching of CoFeB thin films using pulse-modulated high density plasma
CCP	10^{15}	Ar	30 -> 500	An investigation of the spectral lines of argon discharge with Low electron density
2.45 GHz MW	10^{14} -> 10^{17}	He,Ar,O_2,Air	10 -> 90	Characterization of a low-pressure microwave collisional-type coaxial plasma source used for decontamination in food
CCP/ICP	10^{15} -> 10^{17}	Ar	60 -> 600	Optical emission spectroscopy and collisional-radiative modeling for low temperature Ar plasmas
Pulsed ICP	10^{16} -> 10^{17}	Ar, CF_4	1 -> 80	Complex transients of input power and electron density in pulsed inductively coupled discharges
Hollow Cathode	10^{15} -> 10^{16}	O_2	450 -> 787.5	Micro-grooving into thick CVD diamond films via hollow-cathode oxygen plasma etching
ICP	10^{16} -> 10^{17}	H_2	2.25 -> 22.5	A global model study of the population dynamics of molecular hydrogen and the generation of negative hydrogen ions in low-pressure ICP discharge with an expansion region: effects of EEPF
MAGPIE	10^{18}	Ar	3	Wave modeling in a cylindrical non-uniform helicon discharge
ICP	10^{15}	Ar,H_2	40	Absolute density measurement of hydrogen atom in inductively coupled Ar/H2 plasmas using vacuum ultraviolet absorption
CCP	10^{14}-> 10^{15}	Ar	50	Experimental and numerical investigations of the phase-shift effect in capacitively coupled discharges
Magnetron	10^{16}-> 10^{17}	Ar, Ne Kr, Xe	5	Measurements of sputtered neutrals and ions and investigation of their roles on the plasma properties during rf magnetron sputtering of Zn and ZnO targets
CCP (Plasmalab System 100)	0.1 -> 2 Am^{-2}	Ar	2	Ion energy distribution measurements in rf and pulsed dc plasma discharges
Hollow Cathode	10^{16}	Ar	112.5 -> 412.5	Broadband microwave characteristics of a novel coaxial gridded hollow cathode argon plasma
Glow Discharge	10^{16} -> 10^{17}	He	112.5 -> 562.5	Properties of a large volume glow discharge helium plasma by measuring the broadband microwave phase shift in different pressures
CCP	10^{15} -> 10^{16}	H_2,Ar	112.5 -> 1725	Electrical Characteristics of Capacitive Coupled Radio Frequency Discharges in Argon and Hydrogen
CCP	10^{15}	Ar,H_2	585 -> 825	Optical and electrical properties of capacitive coupled radio frequency Ar-H2 mixture discharge at the low pressure
CCP	10^{14} -> 10^{15}	He	120 -> 180	Room temperature photoluminescence in plasma treated rutile TiO2 (110) single crystals
2.45GHz ECR	10^{14} -> 10^{15}	Air	7.5	Investigation of bacterial spore inactivation using a 2.45 GHz coaxial plasma source
CCP	10^{15} -> 10^{18}	Ar	0.45	Collisional radiative modeling on optical emission spectroscopy for Ar plasma
CCP	10^{15} -> 10^{16}	He,Ar,O_2	225 -> 375	Evolution of plasma parameters in capacitively coupled He–O2/Ar mixture plasma generated at low pressure using 13.56 MHz generator
Hollow Cathode	10^{16}	Ar	150	Absolute continuum intensity diagnostics of a novel large coaxial gridded hollow cathode argon plasma
ICP	10^{16} -> 10^{17}	He	0.5 -> 2	Spatial distributions of plasma parameters in inductively coupled hydrogen discharges with an expansion region
CCP	10^{16} -> 10^{18}	He	750	Density, temperature and magnetic field measurements in low density plasmas

MW	10^{16} -> 10^{17}	Ar,O_2	75 -> 225	Heating power at the substrate, electron temperature, and electron density in 2.45 GHz low-pressure microwave plasma
ICP	10^{16} -> 10^{17}	H_2	0.75 -> 37.5	Experimental and numerical investigations of electron characteristics in 2 MHz and 13.56 MHz inductively coupled hydrogen plasmas with an expansion region
CCP	10^{17} -> 10^{18}	Ar	1500	In-Flight Size Focusing of Aerosols by a Low Temperature Plasma
CCP	10^{18}	Ga,Ar,N_2	4200	Nonequilibrium plasma aerotaxy of size controlled GaN nanocrystals
ICP	N/a	CO_2,Ar,N_2	37.5 -> 1312	Tuning of Conversion and Optical Emission by Electron Temperature in Inductively Coupled CO2 Plasma
CCP	10^{14} -> 10^{15}	Ar,C	7.5	Observation of self-excited dust acoustic wave in dusty plasma with nanometer size dust grains
CCP	10^{16}	He,Air	915	The smooth effect of fast electron detection in the positive column in DC glow discharge
HiPIMS (PLATTIT π)	10^{16} -> 10^{17}	Ar, Ti	4.9	Microstructure-driven strengthening of TiB2 coatings deposited by pulsed magnetron sputtering
CCP	10^{16} -> 10^{17}	Ar	20	Control of ion energy distributions using phase shifting in multi-frequency capacitively coupled plasmas
MAGPIE	10^{17} -> 10^{19}	Ar,H_2	3.1	Design and characterization of the Magnetized Plasma Interaction Experiment (MAGPIE): a new source for plasma–
MAGPIE	10^{16}	H_2,N_2	10	A volume-averaged model of nitrogen–hydrogen plasma chemistry to investigate ammonia production in a plasma-
ICP	10^{16} -> 10^{17}	N_2	2.25	The discharge characteristics in nitrogen helicon plasma

*Click here to read more about Langmuir Probe System

*Click here to download the brochure.

PLATO PROBE SYSTEM

The Plato Probe is a planar Langmuir Probe designed to work in deposition plasmas when an insulating film will be deposited on the probe surface. This allows the plasma parameters such as plasma density, Ion current density and electron temperature to be measured in systems where a standard Langmuir probe would not be suitable, such as plasma enhanced chemical vapour deposition (PECVD) systems.

Plasma Source	Electron Temperature (eV)	Gases	Pressure	Published Paper
Ion Beam Assisted-CVD	2-4.5	Ar	0.24 - 1	Ion beam assisted chemical vapor deposition of hybrid coatings—Process diagnostics and mechanisms

*Click here to read more about Plato Probe System.

*Click here to download the brochure.

Impedans Ltd

Chase House

City Junction Business Park, Northern Cross

Dublin - D17 AK63, Ireland

Tel: +353 1 842 8826

Email: sales@impedans.com